ELSEVIER

Surface Science 476 (2001) 139–151

SURFACE SCIENCE

www.elsevier.nl/locate/susc

Underpotential deposition of Cu on iodine-modified Au(1 1 1): an in situ scanning tunneling microscopy study

A. Martínez-Ruiz [a,b], J. Valenzuela-Benavides [c,*], L. Morales de la Garza [c], N. Batina [d]

[a] *Facultad de Ciencias, Universidad Autónoma de Baja California, A.P. 1820, Ensenada, BC 22800, Mexico*
[b] *Centro de Investigación Científica y de Educación Superior de Ensenada, A.P. 2732, Ensenada, BC 22800, Mexico*
[c] *Centro de Ciencias de la Materia Condensada, Universidad Nacional Autónoma de México, A.P. 2681, Ensenada, BC 22800, Mexico*
[d] *Universidad Autónoma Metropolitana-Iztapalapa, A.P. 55-534, C.P. 09340, Mexico, DF, Mexico*

Received 12 May 2000; accepted for publication 7 December 2000

Abstract

The electrochemical deposition of Cu on iodine-modified Au(1 1 1) surfaces has been investigated by in situ electrochemical scanning tunneling microscopy (ECSTM) and cyclic voltammetry (CV) in sulfuric acid solutions. In situ ECSTM studies reveal different iodine adlayer structures before and during the process of copper underpotential deposition (UPD). At the beginning of the cathodic scan and for potentials higher than the onset of UPD a c($p \times \sqrt{3}R$-30°) iodine structure is observed on wide terraces. For lower potentials this iodine structure transforms to a more compact (3×3) structure characterized by two different structural variations (symmetric and asymmetric) sometimes observed coexisting in the same terrace. Charge transfer analysis from CV measurements reveals that the amount of copper deposited at these potentials is not sufficient to account for this structure in the framework of a hard-ball structural model.

During the UPD process itself other iodine structures are also observed as a function of copper deposition, together with an additional compression of the iodine adlayer associated with the formation of a CuI bilayer, in agreement with previously reported X-ray diffraction data. At the end of the UPD process a Cu(1×1) monolayer is formed with a lattice parameter equal to that of Au(1 1 1). The same course of structural changes was also observed during the anodic scan where stripping of the copper layer takes place, returning to the initial iodine c($p \times \sqrt{3}R$-30°) structure. Our results strongly suggest that the iodine adlayer is constantly present as the top layer during the process of electrodeposition and stripping of Cu with no noticeable loss of iodine in the process. The observed structures are discussed in terms of iodine–copper interactions.

Keywords: Electrochemical methods; Scanning tunneling microscopy; Chemisorption; Surface structure, morphology, roughness, and topography; Copper; Gold; Iodine; Solid–liquid interfaces

1. Introduction

In situ electrochemical scanning tunneling microscopy (ECSTM) has become a powerful tool in modern electrochemistry in the past decade, with

* Corresponding author. Address: CCMC-UNAM, P.O. Box 439036, San Ysidro, CA 92143-9036, USA. Tel.: +52-61-74-46-02; fax: +52-61-74-46-03.
E-mail address: valenzue@ccmc.unam.mx (J. Valenzuela-Benavides).

0039-6028/01/$ - see front matter
PII: S0039-6028(01)00691-4

its unique ability of real time imaging of processes occurring on the electrode/electrolyte interface under potential control [1]. A subject that has received much attention is the underpotential deposition (UPD) of metals: a mechanism which occurs at potentials more positive than the Nernst equilibrium potential. Reported studies have clearly demonstrated that the UPD process itself is very sensitive to the structure and nature of the substrate and to the presence of other adsorbed species [2–4]. For example, iodine covered surfaces of Pt, Rh, Pd, Ag and Au show a different electrochemical behavior compared to the clean surface. But perhaps the most studied processes are the UPD of Ag and Cu on clean and iodine-modified Pt(1 1 1) and Au(1 1 1) surfaces, both in sulfuric and perchloric acid solutions [5–16]. These systems have been used as models to further understand the kinetics of metal deposition onto modified surfaces and the influence other modifiers have on the quality and structure of the formed deposits. Moreover, the use of iodine as a surface modifier is important from the technological point of view, since iodine adlayers protect sensitive metal surfaces from oxidation and contamination in ambient conditions, therefore facilitating the handling and preparation of single crystal substrates [17,18].

A particular example of an ECSTM study in this field is the UPD of Ag on Au(1 1 1), where cyclic voltammetry (CV) has shown that deposition is a three-step process. Researchers reported the observation of a $(\sqrt{3} \times \sqrt{3})R30°$ structure after the first UPD peak and a (1×1) structure after the third peak in a H_2SO_4 solution [5]. In contrast, a (4×4) structure was reported for the same system after the first UPD peak in $HClO_4$ and HF solutions, suggesting that neither ClO_4^- or F^- anions are as strongly attached to the Au(1 1 1) surface as the sulfate anion [19]. Moreover, Gewirth and coworkers reported a (3×3) structure after the first UPD peak in a H_2SO_4 solution with AFM [20].

For iodine-modified Au(1 1 1) surfaces, UPD of Ag also takes place in three steps in a $HClO_4$ solution. A $(5 \times \sqrt{3})$ structure was reported before the first UPD peak, corresponding to an iodine coverage of $\theta_I = 0.40$ of a monolayer (ML), followed by the formation of a (3×3) structure after the first peak with equal coverage of I and Ag of 4/9 ML, with iodine as the top layer [8].

Similar studies can be found in the literature for Cu on Pt(1 1 1) and I–Pt(1 1 1), but there are conflicting reports about the observed structures [21–23]. These examples demonstrate that although cyclic voltammograms for bare and iodine-modified metal surfaces appear similar, the surface structures formed can be markedly different.

There are also a considerable number of studies about Cu electrodeposition on clean Au(1 1 1) surfaces. In early work, UPD of Cu on Au(1 1 1) in sulfuric acid solution was thought to form a $(\sqrt{3} \times \sqrt{3})R30°$ structure with a $\theta_{Cu} = 1/3$ ML after the first UPD peak [2,10]. But recent surface X-ray scattering (SXS) studies have confirmed a honeycomb structure for copper ($\theta_{Cu} = 2/3$ ML) with sulfate coadsorption after the first UPD peak, and completion of the full monolayer only after the second UPD peak [24,25]. This is a good example of the importance of using complementary techniques such as traditional electrochemical analysis, LEED, STM and SXS, to better characterize a surface.

In this work we present structural (ECSTM) and electrochemical (CV) studies of UPD of Cu on iodine-modified Au(1 1 1) surfaces in a 0.05 M H_2SO_4 + 1 mM $CuSO_4$ solution, in order to better understand the mechanism of metal electrodeposition in the presence of an adsorbed species.

2. Experimental details

Solutions were prepared using H_2SO_4 (Suprapure, Merck), $CuSO_4$ (Puratronic 99.999%, Alfa Æsar), KI (Puratronic 99.999%, Alfa Æsar) and high resistivity ultrapure water (Millipore-Q).

For the preparation of the gold working electrode, the flame annealing method reported in the literature [26] was followed using commercially available polycrystalline gold thin films evaporated onto a borosilicate glass precoated with a 1–4 nm thick chromium layer to increase adhesion (MHS-GmbH, Germany). After the film was annealed in a H_2 flame for about one minute and cooled in a N_2 gas flow, the iodine adlayer was deposited by immersing the substrate in a 1 mM KI solution for

three minutes at ambient temperature then rinsing in a 0.1 M H_2SO_4 solution. The gold electrode was quickly transferred to the electrochemical cell and immersed in a 0.05 M H_2SO_4 + 1 mM $CuSO_4$ solution at a fixed potential of 0.35 V (versus reference electrode), where CV was performed with a BAS-100 potentiostat (Bioanalytical Systems) using clean copper and platinum wires as quasi-reference and counter electrodes, respectively. In situ ECSTM studies were done with a NanoScope III Electrochemical STM (Digital Instruments), equipped with a specially built Kel-F electrochemical mini-cell open to ambient conditions. Tunneling tips fabricated from tungsten wire were electrochemically etched and coated with nail polish to reduce leakage current. Typical tunneling current used in the experiments ranged from 1 to 20 nA, with tip potential adjusted in order to minimize electrochemical currents. All potentials are referred to the Cu/Cu^{++} quasi-electrode potential.

3. Results and discussion

3.1. Cyclic voltammetry measurements

It has been shown numerous times that well annealed gold thin films possess a good (1 1 1) surface suitable for use as working electrodes, instead of the much more expensive single crystal [4,12]. With this in mind, we first tested the crystallinity of the flame-annealed film by performing CV on our bare Au(1 1 1) electrodes in a 0.05 M H_2SO_4 + 1 mM $CuSO_4$ solution and compared the results with the well-known voltammogram of Cu UPD on a Au(1 1 1) single crystal for the same electrolyte [2–4,10,27]. The resulting voltammogram shown in Fig. 1 is very similar to the one reported for a gold single crystal electrode [27]. As described before, two distinctive adsorption peaks were observed during the cathodic scan, corresponding to a Cu deposition of 2/3 and 1/3 ML after the first and second peak respectively [2, 10,24,25].

For comparison, Fig. 2a shows the voltammogram for Cu UPD on iodine-covered Au(1 1 1), recorded in the same iodine-free 0.05 M H_2SO_4 + 1 mM $CuSO_4$ solution as for the CV in Fig. 1.

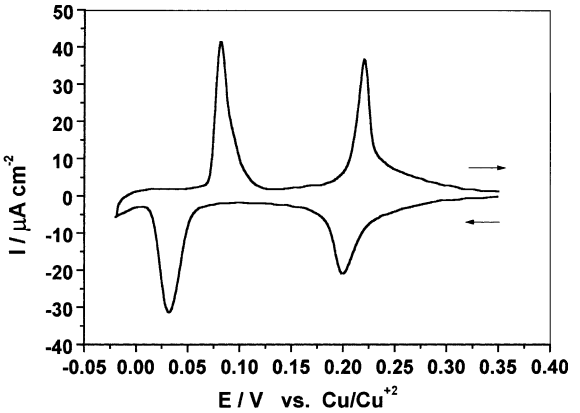

Fig. 1. Cyclic voltammogram of a flame-annealed Au(1 1 1) electrode in 0.05 M H_2SO_4 + 1 mM $CuSO_4$ solution, taken at a scan rate of 5 mV/s.

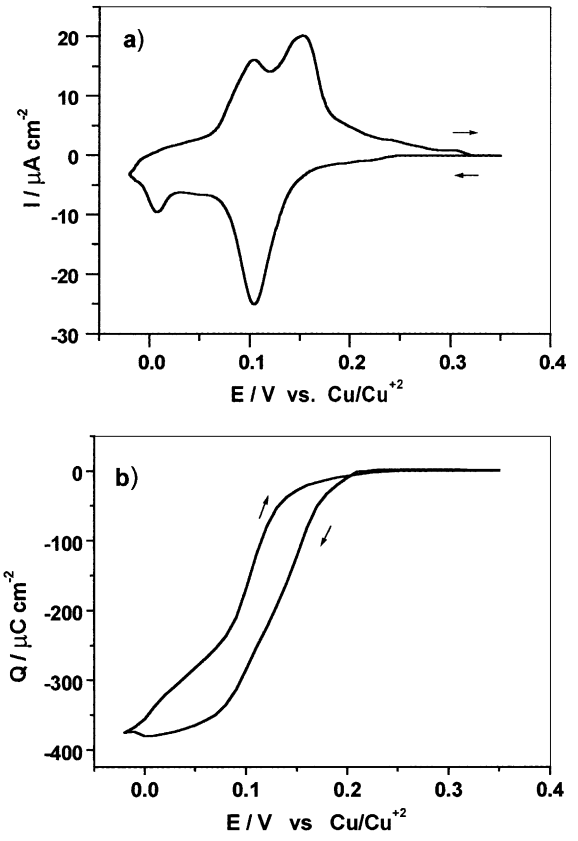

Fig. 2. (a) Cyclic voltammogram of iodine-modified Au(1 1 1) surface in 0.05 M H_2SO_4 + 1 mM $CuSO_4$ solution and (b) coulometric curve. The scan rate was 5 mV/s.

It resembles the voltammogram for Cu UPD on bare Au(1 1 1) in the sense that Cu deposition also takes place via a two-step process. Two distinct reduction peaks with their corresponding oxidation peaks can be recognized for copper adsorption onto the I–Au(1 1 1) surface: a first peak at around 0.105 V and a second but smaller peak at 0.010 V, just before the onset of bulk deposition. When these results are compared with the voltammogram for Cu UPD on a bare Au(1 1 1) surface, it is evident that the deposition peaks are shifted towards less positive potentials. Repeated scan cycles had no significant effect on the shape of the voltammogram. The coulometric curve in Fig. 2b shows that for potentials more positive than 0.25 V no noticeable charge transfer is detected before the first UPD peak. The estimated amount of charge consumed after the first peak was approximately 330 $\mu C/cm^2$, and 50 $\mu C/cm^2$ for the second peak, with a total consumed charge of approximately 380 $\mu C/cm^2$, lower than the expected value of 440 $\mu C/cm^2$, assuming the formation of an epitaxial (1×1) layer of Cu on Au(1 1 1) with a two-electron transfer per Cu atom. However, one must be careful in estimating metal coverages in a UPD processes using charge density calculations by integration of the voltammogram, since the charge density can be scan rate dependent [8]. Nevertheless, it is clear that most of the Cu deposition took place during the first peak on iodine-modified Au(1 1 1), with only a small fraction of a monolayer deposited after the second UPD peak. Apparently sulfate coadsorption is no longer favorable in the presence of the iodine adlayer in order to stabilize the copper structure, as in the case for the bare Au(1 1 1) surface. This point will become clearer when in situ STM results are presented below.

The influence of the scan rate (v) on the shape of the voltammogram was also investigated in detail, since it is well known that Cu UPD on bare Au(1 1 1) is a slow process. It was found that the current density of the first cathodic peak was proportional to v up to 5 mV/s, then proportional to $v^{1/2}$ up to 25 mV/s, after which it becomes independent of scan rate for $v > 25$ mV/s. This result differs from the behavior of Cu UPD on clean Au(1 1 1) in the high scan rate regime, where the current density is proportional to $v^{1/2}$ even for v up to 100 mV/s. A peak shift towards more positive potentials for slower scan rates was also observed, but even for $v = 1$ mV/s the voltammogram showed no significant amounts of copper deposition in the potential region more positive than 0.25 V.

3.2. In situ ECSTM before UPD

The iodine-modified Au(1 1 1) electrode was immersed in the ECSTM cell at a fixed potential of 0.350 V, considerably more positive than the onset of the UPD process. After allowing for thermal drift to settle to an acceptable level, images like the one in Fig. 3 were acquired in large areas of the sample. At this potential the iodine adlayer appears flat with no noticeable vacancies. The measured atomic corrugation amplitude was approximately 0.06 nm with all atoms having equal height. Careful measurements of iodine's interatomic distances averaged over several images

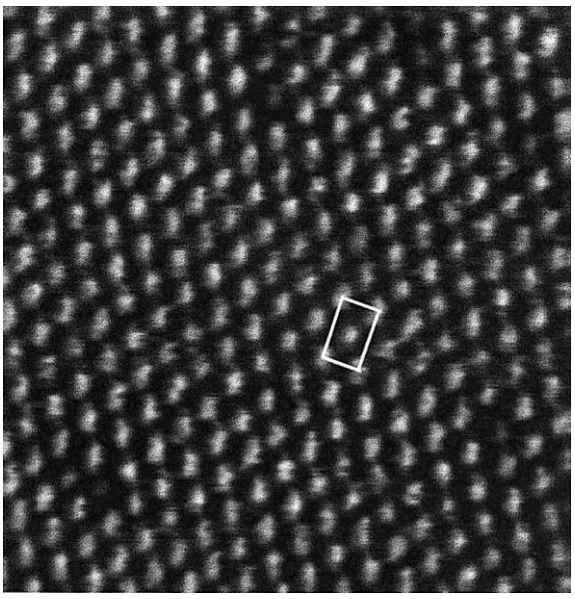

Fig. 3. An unfiltered 7.2×7.2 nm^2 STM image of the c($p \times \sqrt{3}R$-30°) iodine structure taken at $E = 0.35$ V. The z corrugation is approximately 0.05 nm. $I_t = 17$ nA, $E_{tip} = 0.022$ V.

yielded a value of 0.46 nm in two atomic row directions and 0.50 nm for the third atomic row direction, which are in good agreement with the p and $\sqrt{3}$ sides respectively of the well known incommensurate centered rectangular c($p \times \sqrt{3}R$-30°) structure, with $p \cong 2.7$ and a corresponding iodine coverage of $\theta_I = 0.37$ ML. This structure was expected based on previously published work, where potential-dependent magnitude variations of the parameter p were reported, varying from approximate values of 2.5–3: a phenomenon known as "uniaxial compression" [12,28–30]. In the c($p \times \sqrt{3}R$-30°) structure iodine atomic rows are rotated almost 26° with respect to the gold [1 $\underline{1}$ 0] direction, with iodine atoms occupying equivalent sites on the Au(1 1 1) substrate, thus explaining the flatness of the adlayer in our STM images [12].

After lowering the potential to less positive values the c($p \times \sqrt{3}R$-30°) slowly transforms to another structure (Fig. 4a). It appears around 0.320 V and it is observable for potentials as low as 0.240 V, before the onset of the first UPD peak. The image in Fig. 4a reveals six bright spots surrounding a darker spot, with a nearest neighbor distance of 0.43 nm in all three directions and a corresponding coverage of 0.44 ML. The iodine atomic rows are now aligned with the substrate, showing two different corrugation patterns along the rows labeled A and B. For rows of type A, all atoms are of equal height with an average corrugation amplitude of 0.06 nm, whereas along rows of type B the average height difference between alternating bright and dark spots is 0.04 nm. On some occasions domains with a slightly different structure were observed coexisting on the same terrace (Fig. 4b), which can be characterized by four bright spots occupying the corners of the unit cell with darker spots on the sides and in the center. The two images in Fig. 4 present a contrast pattern like a perfect inverse of each other.

In accordance with the measured nearest neighbor interatomic distance and the orientation of the iodine adlayer with respect to the gold lattice, we assigned a (3 × 3) structure to these images [31,32]. Since the (3 × 3) is a more compact structure than the previous c($p \times \sqrt{3}R$-30°), vacancies must appear in the iodine adlayer as a consequence of a reduced iodine–iodine distance, since no additional iodide is available in solution [8]. As seen in both images in Fig. 4, vacancies in the iodine adlayer are in fact observed: as single atom vacancies (Fig. 4b) and as a vacancy island (bottom of Fig. 4a). When the electrode potential

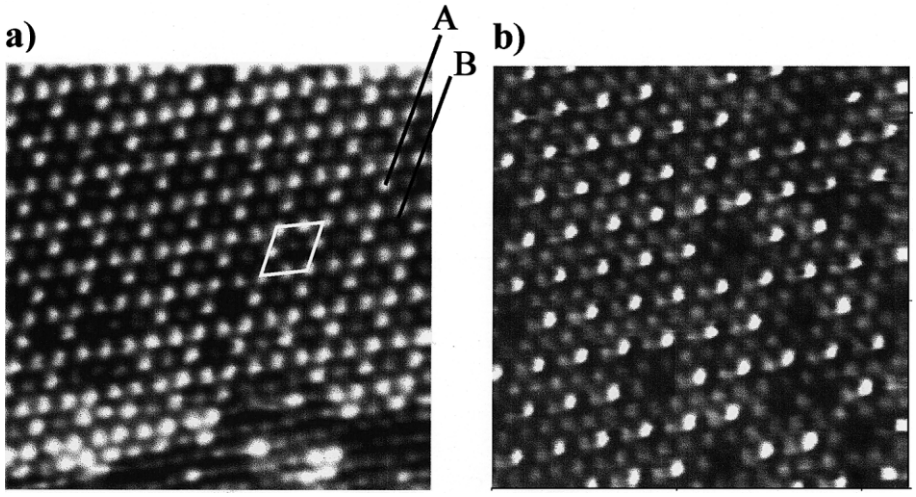

Fig. 4. Filtered 7.2 × 7.2 nm^2 STM images of the (3 × 3) (a) asymmetrical and (b) symmetrical iodine structures with their respective unit cells taken at $E = 0.32$ V. The z corrugation in (a) is 0.06 nm along the row A and 0.04 nm for the alternating bright–dark spots along row B. $I_t = 17$ nA, $E_{tip} = 0.022$ V.

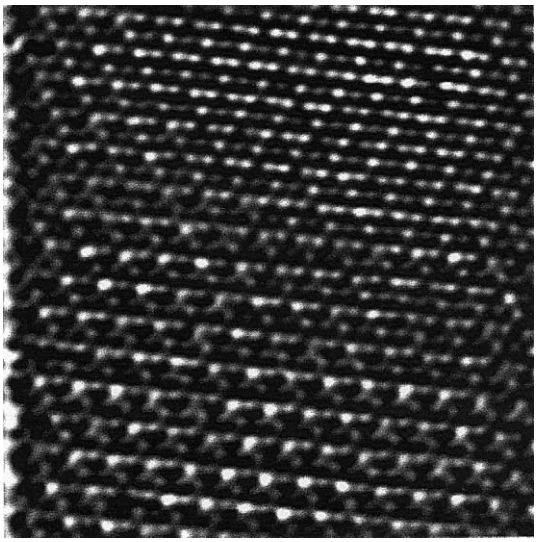

Fig. 5. Filtered 12×12 nm^2 STM image taken at $E = 0.30$ V, it shows both (3×3) symmetrical (lower half) and asymmetrical (upper half) iodine structures coexisting.

is returned to the initial value of 0.350 V, the c($p \times \sqrt{3}R$-30°) structure is again observed as a flat adlayer with no holes or vacancy islands.

The image in Fig. 5 presents two (3×3) domains coexisting in the same Au(1 1 1) terrace, where the upper and lower half structures are similar to the ones shown in Fig. 4a and b respectively. It was also found during the course of the experiments that the structure in Fig. 4a is predominantly obtained if the potential is slowly lowered towards a less positive value, while the structure in Fig. 4b can be easily obtained when the potential is changed abruptly during the imaging process. A possible explanation for this difference is that in the former case, the iodine adlayer goes through a process of layer relaxation when converting from a c($p \times \sqrt{3}R$-30°) to a (3×3) structure, while in the latter case the iodine layer is "forced" to a less relaxed structure. Surely theoretical calculations on the dynamics of such structural transitions are needed in order to better understand the process. Nevertheless, the coexistence of these two (3×3) domains observed in the experiments can be explained by the simple hard-ball model shown in Fig. 6, previously reported for the interpretation of STM images of iodine adlayers on Pt(1 1 1) [6,32]. For the model shown in Fig. 6a, known as (3×3)-asymmetric structure, there are four iodine atoms per unit cell: three in asymmetric on-top sites and one in a threefold hollow site. Such positions can be associated with the height differences seen in the STM images: atoms located in asymmetric on-top sites are higher than the ones located in the threefold hollow site. Therefore, we assigned the image in Fig. 4a to the (3×3)-asymmetric model, and since

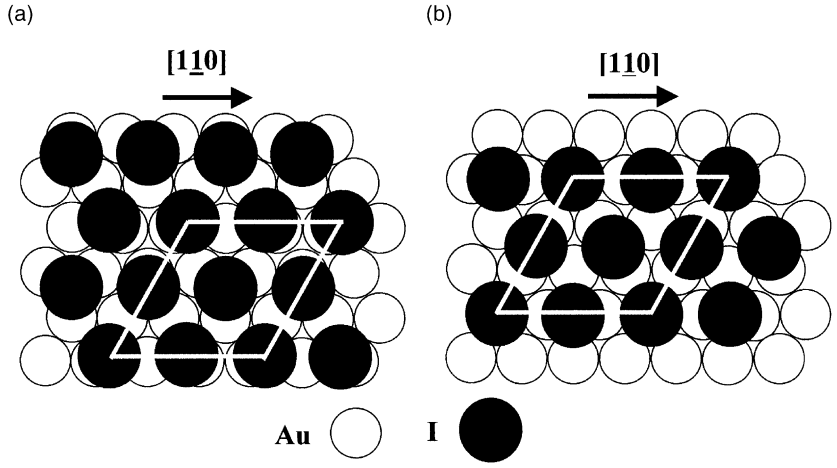

Fig. 6. Hard-ball models of the (3×3) (a) asymmetrical and (b) symmetrical structures. In (a) asymmetric on-top atoms in the corners of the unit cell are higher than the threefold site atom in the center. In (b) on-top corner atoms are higher than the twofold bridge site atoms.

there are four iodine atoms per nine gold atoms in a unit cell, the iodine coverage for this structure is 0.44 ML. Furthermore, in the (3×3)-symmetric model of Fig. 6b the unit cell has a single iodine atom located in an on-top site together with three iodine atoms in equivalent twofold bridge sites, again with the same iodine coverage of 0.44 ML. Comparing the STM image in Fig. 4b with this structural model, the bright spots (higher height) correspond to the on-top corner balls of the unit cell and the darker spots (lower height) to the twofold positions. From purely geometrical considerations, the height difference between hard balls (gold radius $r_{Au} = 0.144$ nm, iodine radius $r_I = 0.215$ nm [33]) in an on-top site and a twofold site is 0.030 nm [12], which roughly agrees with the measured corrugation of $\Delta z = 0.05$ nm in Fig. 4b. The discrepancy can be attributed to electronic (local density of states) effects that make up an STM image, since the contribution to the tunneling current from an iodine atom in an on-top position is different from one iodine atom in a twofold position, as observed in the case of iodine on Pt(1 1 1) [6]. The same arguments can be applied between an on-top asymmetric site and a threefold hollow site, where iodine in the latter sites has intrinsically weaker electron tunneling than on-top, which shows evidence of more efficient tunneling properties. The resulting effect would be a higher value for the measured corrugation amplitude, as is the case in our STM measurements.

Notice from the models in Fig. 6 that the only difference between the symmetric and asymmetric structures is a small lateral displacement of the iodine adlayer with respect to the Au(1 1 1) lattice, i.e., by displacing laterally the symmetric iodine adlayer by a fraction of the gold lattice parameter, the asymmetric structure is obtained, and vice versa. This fact may explain the observed coexistence of the two structures by STM.

To our knowledge the transition to a (3×3) structure under these experimental conditions has not been reported. However, in a previous experiment researchers reported the observation of a (3×3) structure when Cu and I ions from solution were coadsorbed on a Au(1 1 1) surface, but only when the copper coverage reached 0.4 ML [9]. Our CV and coulometric data in Fig. 2 show a very small amount of charge transfer in the range of potentials where the (3×3) structure is observed, thus implying that the STM images in Fig. 4 cannot be attributed to the deposition of copper in the coverages reported in Ref. [9], at least in the framework of a hard-ball structural model.

3.3. In situ ECSTM during UPD

For potentials below 0.20 V the deposition of Cu initiates, forming isolated islands or patches and causing the (3×3) iodine structure with its characteristic atomic corrugation to slowly disappear, revealing a complete hexagonal flat adlayer when a 0.12 V potential is reached. At this potential, the coulometric curve in Fig. 2b indicates a charge density transfer of approximately 200 μC/cm^2, which corresponds to a copper coverage of ~0.45 ML, assuming a charge transfer of two electrons per Cu atom through the interface, even though there is a coadsorbed iodine layer [34,35].

Fig. 7a shows an STM image representative of this structure. Its orientation is the same as the previous (3×3) but appears to be more compact, with a higher density of atomic vacancies on the electrode surface. Careful measurements indicate a small decrease of approximately 5% in the iodine's interatomic distance, changing from the previous value of 0.43 nm for the (3×3) structure to an approximate value of 0.41 nm, which from geometrical considerations a 0.49 ML coverage can be estimated. The slight compression of the iodine layer associated with the deposition of copper explains the observed additional vacancies on the surface, which range from 0.04 to 0.10 nm in depth, lower than the expected value for an iodine layer atomic step. Although the atomic structure inside the pits could no be resolved, the low depth values can be attributed to small amounts of copper present in the pits or to tip geometry.

The measured decrease in iodine's nearest neighbor distance to a value lower than its van der Waals diameter (0.43 nm) [33] cannot be explained by a simple iodine–iodine interaction. As pointed out by Ocko and coworkers, repulsive interaction between the iodine atoms appears to prevent further compression beyond the van der Waals limit

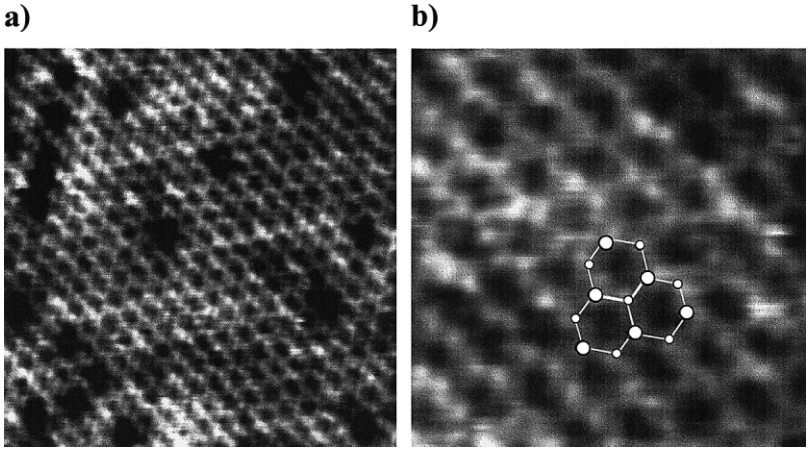

Fig. 7. Filtered STM images taken at $E = 0.12$ V where the CuI bilayer has formed. (a) 7.2×7.2 nm^2 area showing the presence of pits and (b) a higher resolution 2.8×2.8 nm^2 image with a superimposed hexagonal lattice of the CuI structure. The assignment of the Cu (small circles) and I (large circles) on the lattice is arbitrary. $I_t = 17$ nA, $E_{tip} = 0.022$ V.

[36]. Therefore an additional interaction between the iodine layer and the deposited copper has to be responsible for the compression. Moreover, as observed for Pt(1 1 1) [34,35] and Au(1 1 1) electrodes [37,38], even small amounts of deposited copper (below 0.5 ML) enhance the adsorption of halide anions in solution by lowering the surface work function, which explains the observed increase in surface coverage that leads to a compression of the halide adlayer.

In a reported experiment using in situ grazing incidence X-ray scattering and electrochemical techniques with Br adlayers on Au(1 1 1), it was proposed that at the beginning of deposition the copper atoms are mixed in the bromide adlayer, sometimes occupying interstitial holes in the (4×4) structure and promoting the adlayer compression by increasing bromide coverage. With further deposition, the adsorbed copper begins to lift the bromide layer upward as the copper layer moves closer to the Au(1 1 1) surface, leading to the formation of a stoichiometric CuBr bilayer [37]. Such bilayer formation has also been proposed for CuBr on Pt(1 1 1) [35] and on Au(1 1 1) [38], for CuCl on Pt(1 1 1) [39,40] and on Au(1 1 1) [41], and for CuI on Pt(1 1 1) [23, 42], with structures identical to the zinc-blende structure of bulk crystals. For all cases of CuX (X = I, Br, Cl) bilayer structures on Pt(1 1 1) and Au(111), the measured halide–halide interatomic distance is consistently smaller by 3–7% than its corresponding distance in the CuX bulk crystal.

From the aforementioned reported data, together with the estimated and approximately equal coverages of 0.45 and 0.49 of a monolayer of copper and iodine respectively, we have assigned the observed STM images in Fig. 7 to a CuI bilayer structure, with iodine occupying the upper plane [23]. The higher resolution STM image in Fig. 7b shows a drawn superimposed hexagonal lattice, where the I (large circles) and Cu (small circles) atomic sites have been arbitrarily assigned relative to the (1 1 1) plane in a cubic zinc-blende structure of CuI [33]. Since the Au(1 1 1) surface has a larger lattice parameter than Pt(1 1 1) ($d_{Au} = 0.289$ nm, $d_{Pt} = 0.278$ nm), the images in Fig. 7 cannot be correctly defined as (3×3) structures like the CuI bilayer on Pt(1 1 1) reported by Hubbard and coworkers [23], even though iodine–iodine distance for CuI for both surfaces is approximately the same (0.41 nm). This fact suggests a relatively weak bonding between the CuI bilayer and the metal substrate.

To better understand the compression mechanism of the iodine layer during the UPD process, careful measurements of iodine's nearest neighbor distance d_{I-I} were performed along atomic row directions in a series of STM images, before and

after deposition and at different electrode potentials. Although it is difficult to measure lateral distances accurately in STM because of thermal drift and scanner nonlinearities, under controlled experimental conditions reliable data can be collected. The measurements for a particular atomic row direction are presented in Fig. 8, with similar results obtained for the other two directions. The graph shows the changing magnitude of d_{I-I} versus electrode potential, from a value of 0.43 nm for $E > 0.22$ V to 0.41 nm for $E < 0.15$ V. It clearly demonstrates the compression of the iodine layer starting at approximately $E = 0.17$ V, where the voltammogram of Fig. 2a indicates the onset of copper deposition. After taking an STM image at the lowest electrode potential (0.08 V), the potential was scanned in the opposite (positive) direction and held at 0.26 V, where a (3×3) structure was again observed. The distance measured at this potential (open square data point) again gave the expected value of $d_{I-I} = 0.43$ nm, thus confirming that the measured decrease in d_{I-I} from our images is not an artifact due to thermal drift or any other effect.

The image presented in Fig. 9 shows a typical structure obtained after further copper deposition, observed at potentials around 0.10 V down to 0.07 V (after completion of the first UPD peak). It is

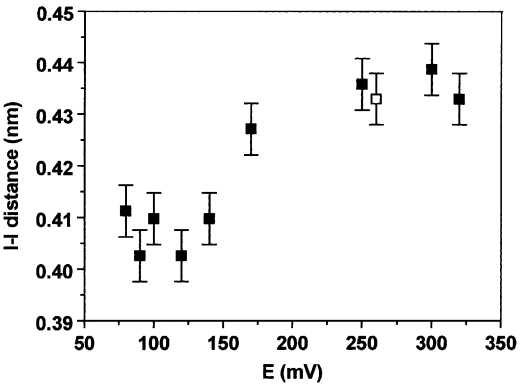

Fig. 8. Iodine–iodine distance versus electrode potential showing iodine adlayer compression during copper deposition. Filled squares data points are from STM images taken during the negative direction of the potential scan. Open square data point is from an STM image taken at the end of the potential scan in the positive direction.

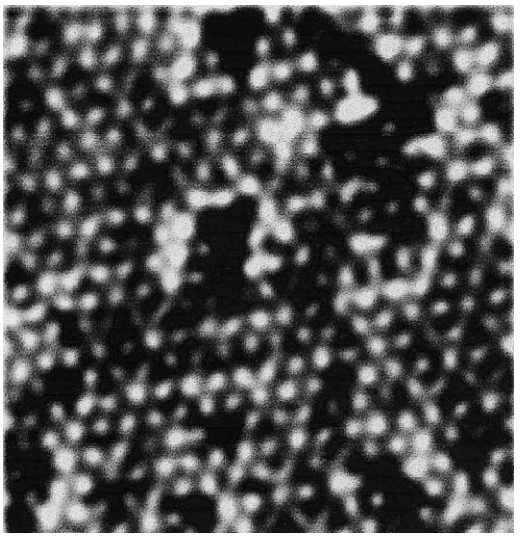

Fig. 9. Filtered 7.2×7.2 nm^2 STM image taken at $E = 0.10$ V of the iodine adlayer with a copper coverage $0.63 < \theta_{Cu} < 0.75$. $I_t = 17$ nA, $E_{tip} = 0.022$ V.

quite different from that in Fig. 7 in several ways: first, the dark center hexagonal structures are no longer present, but instead bright spots associated with iodine atoms are now clearly observed; and second, these bright spots have different intensities, similar to the atomic corrugation seen before on the (3×3) structures. A simple explanation for this effect is as follows: as copper coverage increases together with a decreasing copper–copper distance, the adlayer moves closer to the Au(1 1 1) surface, pushing the iodine adlayer up, in agreement with the "turn-over" mechanism proposed by Markovic and coworkers to explain the process of Cu deposition in the presence of an adsorbed Br adlayer on Pt(1 1 1) [35].

The estimated Cu coverage at this point is between 0.63 and 0.75 ML, in the potential range where structures like the one in Fig. 9 were observed. Slightly similar images were reported by Itaya and coworkers for Ag UPD on I–Pt(1 1 1), but with Ag and I coverages of 0.55 and 0.44 ML, respectively [11].

As the deposition continues towards a complete monolayer coverage of copper, "cracks" in the iodine layer begin to appear, producing isolated patches of ordered iodine structures that eventually disappear when the electrode potential reaches

0.01 V. Fig. 10 shows an STM image taken at $E = 0.005$ V, very near the onset of copper bulk deposition. A complete Cu(1 × 1) monolayer is observed after the second UPD peak and at the end of the UPD process, with the top iodine layer no longer visible. The measured lattice parameter for this Cu epitaxial layer is 0.29 nm, equal to the Au(1 1 1) lattice parameter, but larger than the Cu(1 1 1) lattice parameter of 0.256 nm. The image is interesting because of the apparent absence of the iodine adlayer, and thus requires an description of the imaging mechanism involved. However, as it will be explained below, STM images taken after repeated cycles of copper deposition and stripping indicate that iodine is present at all times on the electrode surface.

Upon reversing the electrode potential to its initial more positive value of 0.350 V, the deposited copper is stripped away from the surface and the iodine's c($p \times \sqrt{3}R$-30°) structure is again formed with no visible holes in the adlayer, thus confirming previous evidence that iodine remains at the surface during the UPD process and with no noticeable amounts dissolved into the solution

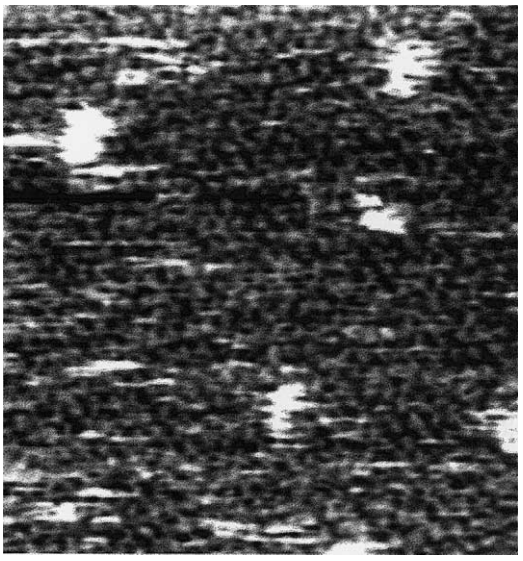

Fig. 10. Unfiltered 7.2×7.2 nm^2 STM image taken at $E = 0.005$ V at the end of UPD near the beginning of bulk deposition. A Cu(1 × 1) structure has formed with lattice parameter equal to gold. $I_t = 23$ nA, $E_{tip} = 0.022$ V.

[8,11,34,35,43]. Of course, if the electrode potential is driven to higher positive values (>1 V) oxidation and stripping of the iodine layer occurs, and after a few cycles complete removal is achieved, revealing a bare Au(1 1 1) surface with its characteristic voltammogram (Fig. 1).

4. Further discussion

To our knowledge the above described phase transition from the c($p \times \sqrt{3}R$-30°) structure to a more compact (3 × 3) structure observed as the potential is changed towards less positive values, has not been previously reported and deserves further discussion.

First, it is useful to review some reported results about the behavior of iodine adlayers on Au(1 1 1) surfaces as a function of electrode potential. By using SXS Ocko and coworkers first revealed the continuous compression of iodine adlayers on Au(1 1 1) as the iodine coverage increases due to changes in the electrode potential in solutions containing iodide, a phenomenon known as "electrocompression" [36]. Two distinct incommensurate iodine monolayer phases where observed: the c($p \times \sqrt{3}R$-30°) structure in the lower potential range and the rotated hexagonal ("rothex") structure at more positive potentials. The transition between these two phases was observed in the positive ("electrocompression") as well as the negative ("electrodecompression") sweep directions. Using STM and LEED, a similar behavior was reported for iodine-modified Au(1 1 1) in perchloric acid solutions [12], and for Au(1 1 1) [29] and Ag(1 1 1) [30] in copper-free aqueous iodide solutions. Whether iodine is electrodeposited from solution or preadsorbed on the surface, the observation of the above mentioned structures are apparently not affected by the nature of the supporting electrolyte, iodide concentration or potential sweep direction.

Our observation of a (3 × 3) structure during the negative scan of the electrode potential (before UPD) is not in accordance with the reported behavior of an iodine adlayer on a Au(1 1 1) surface, although our experiments involved the presence of a different component that could explain our re-

sults: sulfate anions. It is interesting to note that no reports were found on iodine-modified Au-(1 1 1) surfaces in solutions containing sulfate anions. One reference in the literature was found that describes a structural transition from ($\sqrt{3} \times \sqrt{3}$)R30° to the more compact (3×3) structure during iodine adsorption on a Au(1 1 1) surface in a NaI solution [47]. However the image presented by the authors does not show the atomic corrugation expected for a (3×3) iodine adlayer on a Au(1 1 1) surface.

To elucidate whether copper ions in solution play a role in the phase transition process, in situ STM experiments were performed with iodine-modified Au(1 1 1) in pure sulfuric acid solutions. Surprisingly, our preliminary results also revealed the formation of a (3×3) iodine structure under these conditions, with symmetrical and asymmetrical structures observed coexisting in the same terrace. Since electrochemical data indicate that copper coverage is very small in the potential range where the (3×3) structure was found, the results strongly suggest that the observation of the (3×3) iodine structure is more closely related to the presence of sulfates anions than to the presence of copper, hence varying the copper concentration is not expected to play a significant role on the structural transition. However, we cannot totally rule out the effects of small amounts of adsorbed copper on the iodine adlayer structure. Further work is currently underway to corroborate this statement.

Another point that needs further discussion is the ECSTM image taken at the end of the UPD process, where a Cu pseudomorphic layer is observed with no apparent evidence of the presence of the iodine layer. To explain the image in Fig. 10 one should be reminded of the tunneling mechanisms in STM. Although the iodine layer is on top, under particular tunneling conditions it is possible to selectively observe the Cu underlayer by reducing the microscope's tunneling gap resistance R_g below a certain value, around 1 MΩ, either by lowering the bias voltage V_b and/or by increasing the tunneling current I_t ($R_g = V_b/I_t$). On the other hand, by increasing the tunneling gap resistance (typically $\gg 1$ MΩ) the top iodine adlayer can be observed. Surprisingly, many studies have been reported that used this imaging technique [7,12, 32,44–46], the mechanism for such selective imaging is not yet fully understood. In our case, attempts to clearly observe the top iodine adlayer by increasing R_g were unsuccessful, although a very faint structure did emerge that seems to be oriented approximately 30° with respect to the Cu-(1×1) adlayer. In similar studies involving iodine, a c($p \times \sqrt{3}R$-30°) iodine structure was formed after completion of UPD of Cu on I–Pt(1 1 1) [43]. The same c($p \times \sqrt{3}R$-30°) also forms on Au(1 1 1) (as described in the present experiment) and Ag(1 1 1) electrodes [12,28,30]. So we would expect that the same structure would form in our case on top of the Cu monolayer and that our faint image corresponds to this structure, but no clear evidence is presented at this time.

Finally, a summary of most of the available data found in the literature on copper-halide bilayer formation on Pt(1 1 1) and Au(1 1 1) surfaces is presented in Table 1. The data clearly show consistently smaller values for interatomic distances in the bilayer, compared to those of the corresponding bulk zinc-blende structure. The only data that is significantly larger than the expected value for d_{I-I} is from Ref. [9]. The authors reported the observation of a (3×3) structure when Cu coverage reached 0.40 ML in an experiment of Cu and I coadsorption on a Au(1 1 1) surface, with a nearest neighbor distance of 0.43 nm. It is suspected that what they reported as a (3×3) was actually a more compact structure like the one presented in Fig. 7, with $d_{I-I} = 0.41$ nm that could easily be mistaken as a (3×3). In fact, our images look very similar to the one reported in Ref. [9].

5. Conclusions

The UPD of Cu on iodine-modified Au(1 1 1) electrodes in sulfuric acid solution has been investigated using in situ ECSTM and CV techniques. For less positive potentials (before the first UPD peak) the iodine adlayer undergoes a structural transition from a c($p \times \sqrt{3}R$-30°) to a (3×3) symmetrical or asymmetrical structure, sometimes both structures coexisting on the same Au(1 1 1) terrace. Since a (3×3) iodine structure was also

Table 1
Summary of reported data on copper-halide bilayers formed on Pt(1 1 1) and Au(1 1 1) surfaces, together with bulk crystal values for comparison

	θ_{Cu} (ML)	d_{Cu-Cu} or d_{I-I} in bilayer (nm)	d_{Cu-Cu} in bulk[a] (nm)	Substrate	Reference
CuCl	0.62	0.367	0.383	Au(1 1 1)	[41]
	0.585	0.363	0.383	Pt(1 1 1)	[39,40]
CuBr	0.563	0.385	0.402	Au(1 1 1)	[37]
	0.55	0.374	0.402	Pt(1 1 1)	[35]
	0.54	0.378	0.402	Pt(1 1 1)	[40]
CuI	0.44	0.416	0.427	Pt(1 1 1)	[23]
	0.40	0.43[b]	0.427	Au(1 1 1)	[9]
	0.45	0.41	0.427	Au(1 1 1)	This work

[a] Zinc-blende structure.
[b] See text for details.

observed in copper-free sulfuric acid solutions, the structural transition is more likely attributed to a possible interaction between sulfate anions and the substrate within the double layer. Nevertheless, the precise mechanism involved is not fully understood.

Because two (3×3) structures were observed coexisting on the same terrace, a simple hard-ball model suggests that the difference in the atomic corrugation intensities can be explained by a small lateral displacement of the iodine adlayer with respect to the Au(1 1 1) lattice.

Furthermore, CV measurements indicate that UPD of Cu on iodine-modified Au(1 1 1) is a two-step process, similar to that on bare Au(1 1 1), but with UPD peaks displaced towards less positive potentials. During copper deposition a further compression of the iodine adlayer is observed until a CuI bilayer is formed, with copper coverage close to half a monolayer. For higher copper coverages, the STM images suggest that the I adlayer is "pushed-up" by the copper underlayer, in agreement with published X-ray data and the previously proposed "turn-over" model. At the end of the UPD process, a Cu(1×1) layer is observed under special tunneling conditions of a low gap resistance.

Finally, the electrodeposition of Cu is a completely reversible process: it can be stripped from the surface by reversing the potential to higher positive values where the iodine c$(p \times \sqrt{3}R\text{-}30°)$ structure is again observed, indicating that a stable iodine adlayer remains on the surface at all times during the deposition process. Comparing our findings with those for Cu UPD onto a bare Au(1 1 1) surface, it is clear that the deposition mechanism for an iodine-modified Au(1 1 1) surface is a more complex process, dominated by a strong copper–iodine interaction.

Acknowledgements

The authors express their thanks to M. Palomar and N. Takeuchi for many fruitful discussions, and to M. Gould for her help in writing the manuscript. Also to A. Tiznado, O.M. Aguirre, and C. Carballo for their technical support. This work was supported by grants no. 25291-E, 0913E-P and L0081-E9608, from CONACyT. A.M.R. acknowledges a scholarship support and N.B. a Catedra Patrimonial Nivel II, also from CONACyT.

References

[1] A.A. Gewirth, B.K. Niece, Chem. Rev. 97 (1997) 1129.
[2] O.M. Magnussen, J. Hotlos, R.J. Nichols, D.M. Kolb, R.J. Behm, Phys. Rev. Lett. 64 (1990) 2929.
[3] O.M. Magnussen, J. Hotlos, G. Beitel, D.M. Kolb, R.J. Behm, J. Vac. Sci. Technol. B 9 (1991) 969.
[4] N. Batina, T. Will, D.M. Kolb, Faraday Discuss. 94 (1992) 93.
[5] T. Hachiya, K. Itaya, Ultramicroscopy 42–44 (1992) 445.

[6] S.-C. Chang, S.-L. Yau, B.C. Schardt, M.J. Weaver, J. Phys. Chem. 95 (1991) 4787.
[7] W. Haiss, J.K. Sass, X. Gao, M.J. Weaver, Surf. Sci. Lett. 274 (1992) L593.
[8] S. Sugita, T. Abe, K. Itaya, J. Phys. Chem. 97 (1993) 8780.
[9] H. Matsumoto, I. Oda, J. Inukai, M. Ito, J. Electroanal. Chem. 356 (1993) 275.
[10] N. Ikemiya, S. Miyaoka, S. Hara, Surf. Sci. 311 (1994) L641.
[11] N. Shinotsuka, K. Sachikata, K. Itaya, Surf. Sci. 335 (1995) 75.
[12] N. Batina, T. Yamada, K. Itaya, Langmuir 11 (1995) 4568.
[13] A.T. Hubbard, J.L. Stickney, S.D. Rosasco, M.P. Soriaga, D. Song, J. Electroanal. Chem. 150 (1983) 165.
[14] N. Kimizuka, K. Itaya, Faraday Discuss. 94 (1992) 117.
[15] R.J. Nichols, in: A.A. Gewirth, H. Siegenthaler (Eds.), Nanoscope Probes of the Solid/Liquid Interface, NATO ASI Series-288, Kluwer Academic Publishers, London, 1995.
[16] J.G. Xu, X.W. Wang, Surf. Sci. 408 (1998) 317.
[17] A. Wieckowski, S.D. Rosasco, B.C. Schardt, J.L. Stickney, A.T. Hubbard, Inorg. Chem. 23 (1984) 565.
[18] F. Lu, G.N. Salaita, H. Baltruschat, A.T. Hubbard, J. Electroanal. Chem. 222 (1987) 305.
[19] K. Ogaki, K. Itaya, Electrochem. Acta 40 (1995) 1249.
[20] C.-H. Chen, S.M. Vesecky, A.A. Gewirth, J. Am. Chem. Soc. 114 (1992) 451.
[21] K. Sashikata, N. Furuya, K. Itaya, J. Electroanal. Chem. 316 (1991) 361.
[22] I. Oda, Y. Shingaya, H. Matsumoto, M. Ito, J. Electroanal. Chem. 409 (1996) 95.
[23] J.L. Stickney, S.D. Rosasco, A.T. Hubbard, J. Electrochem. Soc. 131 (1984) 260.
[24] Z. Chi, J. Lipkowski, J. Electroanal. Chem. 364 (1994) 289.
[25] M.F. Toney, J.N. Howard, J. Richer, G.L. Borges, J.G. Gordon, O.R. Melroy, Phys. Rev. Lett. 75 (1995) 4472.
[26] W. Haiss, D. Lackey, J.K. Sass, K.H. Besocke, J. Chem. Phys. 95 (1991) 2193.
[27] D.M. Kolb, K. Al Jaaf-Golze, M.S. Zei, DECHEMA-Monographien Bd 102 VCH, Weinheim, 1986.
[28] T. Yamada, N. Batina, K. Itaya, J. Phys. Chem. 99 (1995) 8817.
[29] T. Yamada, N. Batina, K. Itaya, Surf. Sci. 335 (1995) 204.
[30] T. Yamada, K. Ogaki, Sh. Okubo, K. Itaya, Surf. Sci. 369 (1996) 321.
[31] X. Gao, M.J. Weaver, J. Am. Chem. Soc. 114 (1992) 8544.
[32] B.C. Schardt, S.-L. Yau, F. Rinaldi, Science 243 (1989) 1050.
[33] L.P. Pauling. The Nature of the Chemical Bond, Cornell University Press, Ithaca, NY, 1960.
[34] R. Gómez, H.S. Yee, G.M. Bommarito, J.M. Feliu, H.D. Abruña, Surf. Sci. 335 (1995) 101.
[35] N.M. Markovic, Ch.A. Lucas, H.A. Gasteiger, P.N. Ross Jr., Surf. Sci. 372 (1997) 239.
[36] B.M. Ocko, G.M. Watson, J. Wang, J. Phys. Chem. 98 (1994) 897.
[37] E. Herrero, S. Glazier, H.D. Abruña, J. Phys. Chem. B 102 (1998) 9825.
[38] E. Herrero, S. Glazier, L.J. Buller, H.D. Abruña, J. Electroanal. Chem. 461 (1999) 121.
[39] N.M. Markovic, H.A. Gasteiger, Ch.A. Lucas, I.M. Tidswell, P.N. Ross Jr., Surf. Sci. 335 (1995) 91.
[40] I.M. Tidswell, Ch.A. Lucas, N.M. Markovic, P.N. Ross, Phys. Rev. B 51 (1995) 10205.
[41] J. Hotlos, O.M. Magnussen, R.J. Behm, Surf. Sci. 335 (1995) 129.
[42] G.M. Bommarito, D. Acevedo, J.F. Rodríguez, H.D. Abruña, J. Electroanal. Chem. 98 (1994) 5514.
[43] J. Inukai, Y. Osawa, M. Sashikata, Y.-G. Kim, K. Itaya, J. Phys. Chem. B 102 (1998) 3498.
[44] O.M. Magnussen, J. Hagebock, J. Hotlos, R.J. Behm, Faraday Discuss. 94 (1992) 329.
[45] M. Kunitake, N. Batina, K. Itaya, Langmuir 11 (1995) 2337.
[46] K. Ogaki, N. Batina, M. Kunitake, K. Itaya, J. Phys. Chem. 100 (1996) 7185.
[47] N.J. Tao, S.M. Lindsay, J. Phys. Chem. 96 (1992) 5213.